Model Systems for Probing Metal Cation Hydration: The V⁺(H₂O) and ArV⁺(H₂O) Complexes[†]

Veronika Kasalová, Wesley D. Allen,* and Henry F. Schaefer III

Center for Computational Chemistry, University of Georgia, Athens, Georgia 30602-2525

E. Dinesh Pillai and Michael A. Duncan

Department of Chemistry, University of Georgia, Athens, Georgia 30602-2556

Received: February 12, 2007; In Final Form: March 23, 2007

In support of mass-selected infrared photodissociation (IRPD) spectroscopy experiments, coupled-cluster methods including all single and double excitations (CCSD) and a perturbative contribution from connected triple excitations [CCSD(T)] have been used to study the V⁺(H₂O) and ArV⁺(H₂O) complexes. Equilibrium geometries, harmonic vibrational frequencies, and dissociation energies were computed for the four lowest-lying quintet states ($^5A_1$, $^5A_2$, $^5B_1$, and $^5B_2$), all of which appear within a 6 kcal mol⁻¹ energy range. Moreover, anharmonic vibrational analyses with complete quartic force fields were executed for the $^5A_1$ states of V⁺(H₂O) and ArV⁺(H₂O). Two different basis sets were used: a Wachters+f V[8s6p4d1f] basis with triple-ζ plus polarization (TZP) for O, H, and Ar; and an Ahlrichs QZVPP V[11s6p5d3f2g] and Ar[9s6p4d2f1g] basis with aug-cc-pVQZ for O and H. The ground state is predicted to be $^5A_1$ for V⁺(H₂O), but argon tagging changes the lowest-lying state to $^5B_1$ for ArV⁺(H₂O). Our computations show an opening of 2°−3° in the equilibrium bond angle of H₂O due to its interaction with the metal ion. Zero-point vibrational averaging increases the *effective* bond angle further by 2.0°−2.5°, mostly because of off-axis motion of the heavy vanadium atom rather than changes in the water bending potential. The total theoretical shift in the bond angle of about +4° is significantly less than the widening near 9° deduced from IRPD experiments. The binding energies (D_0) for the successive addition of H₂O and Ar to the vanadium cation are 36.2 and 9.4 kcal mol⁻¹, respectively.

I. Introduction

Central to understanding the bulk solvation of metal ions is the interaction of the individual ions and solvent molecules. Metal-cation/water complexes are of the most fundamental interest. However, the details of metal-solvation processes are difficult to determine experimentally, and gas-phase spectroscopic structures of water molecules in contact with a metal cation are rare in the literature.

Photodissociation spectroscopy has been used previously for many metal−ligand complexes to obtain vibrationally resolved spectra for electronic states, as well as rotationally resolved spectra that have provided some of the first direct structural determinations for these molecules. Beginning in the early and mid-1990s, several research groups investigated the electronic spectra of metal-cation/water complexes,[1−11] using size selection with various forms of mass spectrometry and laser photodissociation spectroscopy. In one of the first of these studies, Brucat and co-workers measured a vibrationally resolved electronic spectrum for V⁺(H₂O).[1] Electronic spectra of the alkaline earth cations Mg⁺ and Ca⁺ in complexes with water were studied by Duncan et al.[2−4] and Fuke et al.[5−7] More recently, these studies have been extended to other metals[8] and have included doubly charged ions.[9−11] Duncan and co-workers described the ZEKE photoelectron spectroscopy of Al⁺(H₂O) with partial rotational resolution.[12]

Lisy et al.[13−16] were the first to apply infrared photodissociation spectroscopy (IRPD) to metal-ion/ligand systems, including alkali-cation/water complexes. Beginning in 2002, more extensive mass-selected IRPD studies were executed within the Duncan group on a variety of main group transition-metal/ligand complexes produced by laser vaporization sources.[17−27] In some of the most recent work, these IRPD studies were extended to various M⁺(H₂O)ₙ complexes (M = V, Fe, Ni).[21,25−27] In 2004, Nishi and co-workers[28,29] reported similar studies on Mg⁺(H₂O) and Al⁺(H₂O).

A stronger metal−ligand bond in complexes with a transition metal, as compared with alkali metals,[30−37] makes these systems challenging candidates for spectroscopy. The bond energy of transition-metal-cation/water complexes is too high for single-photon infrared photodissociation; therefore, multiphoton dissociation or "argon tagging" is necessary. The principle behind "argon tagging" is that clusters with rare gas atoms loosely attached have dissociation channels that are accessible at lower photon energies, thus allowing mass spectrometric detection of infrared absorption across wider frequency ranges. It is generally assumed that the argon in such mixed complexes acts as a spectator and does not induce significant structural changes in the clusters or shift the vibrations by substantial amounts.

Recently, the Duncan group applied mass-selected IRPD spectroscopy to the vanadium-cation/water complex.[21] This study provided the first gas-phase IR data on a transition-metal-cation/water system. Vanadium was chosen because it has a single isotope, thus simplifying the mass analysis. Additionally,

7600 *J. Phys. Chem. A, Vol. 111, No. 31, 2007*

Kasalová et al.

the binding energies of V^+ to H_2O or to Ar have been measured previously.[31,32,34,38,39] $V^+(H_2O)$, $V^+(H_2O)Ar_n$, $V^+(D_2O)$, and $V^+(D_2O)Ar_n$ were produced by laser vaporization of a metal target rod and entrainment in an Ar expansion gas. The observation of widely spaced rotational structure indicates that the argon atom attaches to the vanadium cation on the opposite side of the water molecule. After mass selecting the target species, the O–H and O–D stretches in the water moiety were vibrationally excited, and fragment-ion versus energy photo-dissociation spectra were recorded.

The IRPD spectrum of $ArV^+(H_2O)$ contains peaks at 3605 and 3690 cm^{-1}.[21] These bands are $\sim 50\ cm^{-1}$ and $\sim 70\ cm^{-1}$ to the red of the symmetric (3657 cm^{-1}) and antisymmetric (3756 cm^{-1}) stretches in free water, respectively. Scaled vibrational frequencies of $ArV^+(H_2O)$ derived from the B3LYP/6-31G* level of theory (3642 and 3700 cm^{-1}) agree qualitatively with the measured red shifts. For the theoretically predicted $^5B_1$ ground state, the DFT-computed H–O–H angle is 107.5°.

The rotational constants of $ArV^+(H_2O)$, corresponding to the Ar–V–O principal axis, surmised from the profile of the IRPD spectrum of the H_2O antisymmetric stretch were $A' = 7.96\ cm^{-1}$ and $A'' = 12.52\ cm^{-1}$, for the upper ($v_3 = 1$) and lower ($v_3 = 0$) vibrational levels, respectively.[21] The A'' value would indicate an H–O–H angle (113.8°) much more expanded upon complexation than predicted by B3LYP/6-31G* density functional theory. The large difference between A' and A'' would point to a prodigious vibrationally averaged geometry distortion in the complex for the O–H antisymmetric stretching fundamental level.

Prior to the IRPD experiment performed by Duncan's group,[21] the $V^+(H_2O)$ complex was probed by various experimental methods, including collision induced dissociation (CID),[31,32,34] resonant one-photon dissociation spectroscopy,[1] and charge stripping mass spectrometry.[38] The vanadium-cation/water complex showed characteristics of an electrostatically bound species, with a dissociation energy $D_0 = 35 \pm 4$ kcal mol^{-1} (see Table 1) and a V–O stretching frequency $\omega''_e = 420 \pm 75$ cm^{-1}. V^+Ar was studied with electronic spectroscopy by Brucat and Lessen, which provided a binding energy for this system of 8.76 kcal mol^{-1}.[39]

Various computational methods have been applied to $V^+(H_2O)$, including the modified coupled pair functional (MCPF) approach,[40,41] Møller–Plesset perturbation theory,[42,43] configuration interaction,[42] density functional theory,[38,44−46] and limited coupled-cluster methods.[38,43−45] These theoretical studies focused on structures and dissociation energies for the ground state ($^5A_1$) and the lowest-lying ($^5A_2$, $^5B_1$, $^5B_2$) states. Also, it was confirmed that the HV^+OH intermediate, hypothesized by experimentalists,[31] is a well-defined minimum on the potential energy surface, lying 53.8 kcal mol^{-1} above $V^+(H_2O)$.[44] To our knowledge, no theoretical data is available for the $ArV^+(H_2O)$ complex.

Motivated by the IRPD experiments, the $V^+(H_2O)$ and $ArV^+(H_2O)$ complexes are studied here as model systems for metal cation hydration. Accurate structures are obtained for the lowest-lying states of the $V^+(H_2O)$ and $ArV^+(H_2O)$ complexes, and the effects of vibrational averaging on the structures (in particular the H–O–H angle expansion) are analyzed. Definitive dissociation and adiabatic excitation energies are determined as well.

II. Theoretical Methods

To ensure against spin contamination, reference electronic wave functions were determined by the single-configuration restricted open-shell Hartree–Fock (ROHF) method.[47−50] Elec-

TABLE 1: Dissociation Energies for the $^5A_1$ State of $V^+(H_2O)$ in kcal mol^{-1}

	D_e	D_0
present work		
ROHF/Wf(TZP)	37.5	35.8
CCSD/Wf(TZP)	38.1	36.4
CCSD(T)/Wf(TZP)	38.5	36.8
ROHF/QZVPP	35.8	34.2
CCSD/QZVPP	37.6	35.8
CCSD(T)/QZVPP	38.0	36.2
previous theory		
MCPF/Wachters+f TZP^a	36.4	34.7
MP2/6-311++G**^{b}	40.0	
CCSD(T)/6-311++G**//MP2/6-311++G**^{b}	43.4	
B3LYP/TZVP+G(3df,2p)	38.5^c	36.62^d
CCSD(T)/TZVP+G(3df,2p)// B3LYP/TZVP+G(3df,2p)	36.7^c	32.42^d
B3LYP/B3//B3LYP/B2^{ef}		38.7
MPW1PW91/6-311+G(d)^g		35.4
experiment^h		
collision-induced dissociation^i		36.2 ± 3
collision-induced dissociation^j		35.1 ± 4
photodissociation spectrum^k		<45.4
collision-induced dissociation^l		35.8 ± 1.2
compiled in ref 38		35.1 ± 1.2

^{a} References 40 and 41. ^{b} Obtained from the supplementary material of ref 43. The text of the paper reports $\Delta H°_{298} = 38.5$ and 41.8 kcal mol^{-1} from the MP2 and CCSD(T) computations, respectively. ^{c} Reference 38. ^{d} Reference 44. ^{e} B2: 6-311+G* basis for V, 6-31G* basis for O and H; B3: B2 with diffuse s and p functions added to O. ^{f} Reference 45. ^{g} Reference 46. ^{h} Experimental values generally correspond to bond enthalpies at 298 K. ^{i} Reference 31. ^{j} Reference 32. ^{k} Reference 1. ^{l} Reference 34.

tron correlation was then included by the coupled-cluster singles and doubles method (CCSD),[51−54] as well as CCSD with a perturbative contribution from connected triple excitations [CCSD(T)].[54−58] All open-shell coupled-cluster energies were determined from a spin-orbital formulation into which ROHF orbitals were substituted.[54] The 1s, 2s, and 2p core orbitals of vanadium and argon, as well as the 1s core orbital of oxygen, were frozen in the correlation treatments. When investigating the multireference character of $V^+(H_2O)$, state-averaged (SA) complete active space self-consistent field (CASSCF)[59,60] single-point computations were performed with a 12 electron/13 molecular orbital (MO) active space.

Two basis sets were utilized in this study. The smaller basis set, denoted Wf(TZP), was constructed from the Wachters[61] set with supplemental diffuse p, diffuse d, and f-polarization functions[62−64] for vanadium, from the valence triple-ζ basis set of Dunning[65] with added polarization functions (TZP) for oxygen and hydrogen [$\alpha_p(H) = 0.75$, $\alpha_d(O) = 0.85$], and from the Schäfer, Huber, and Ahlrichs TZV[66] basis set with added polarization functions[67] for argon. The final Wf(TZP) contraction schemes are V(14s11p6d3f/8s6p4d1f), O(11s6p1d/5s3p1d), H(5s1p/3s1p), and Ar(14s9p1d/5s4p1d). A larger basis set of quadruple-ζ quality, denoted collectively as QZVPP here, consisted of the QZVPP basis published by Weigend, Furche, and Ahlrichs in 2003 for the vanadium and argon atoms,[68] and Dunning's augmented correlation-consistent polarized-valence quadruple-ζ (aug-cc-pVQZ) basis set[69,70] for oxygen and hydrogen. The final contraction schemes for the QZVPP basis set are V(24s18p9d3f2g/11s6p5d3f2g), Ar(20s14p4d2f1g/9s6p4d2f1g), O(13s7p4d3f2g/6s5p4d3f2g), and H(7s4p3d2f/5s4p3d2f). The QZVPP basis functions for vanadium are designed to have sufficient flexibility in the outer core region to correlate the 3s and 3p electrons.
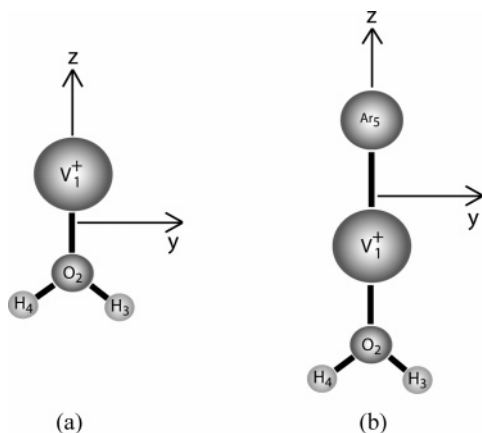
Figure 1. C_{2v} structures of the (a) V$^+$(H$_2$O) and (b) ArV$^+$(H$_2$O) complexes.

Tightly optimized geometrical structures (with all gradient components $<10^{-6}$ au) were obtained at each level of theory. The harmonic vibrational frequencies for the geometric minima of V$^+$(H$_2$O) and ArV$^+$(H$_2$O) were computed for both basis sets with the ROHF, CCSD, and CCSD(T) methods. To determine fundamental frequencies and zero-point vibrational (ZPV) effects on rotational constants, quartic force fields for V$^+$(H$_2$O), ArV$^+$(H$_2$O), and H$_2$O were computed at the Wf(TZP) CCSD and CCSD(T) levels of theory and employed in concert with second-order vibrational perturbation theory (VPT2)[71–75] to determine anharmonic constants. Adopting the atomic labeling of Figure 1, the following symmetry-adapted internal coordinates were utilized for V$^+$(H$_2$O) and ArV$^+$(H$_2$O): $S_1(a_1) = r_{12}$ (V−O stretch); $S_2(a_1) = 2^{-1/2}(r_{23} + r_{24})$ (H$_2$O symmetric stretch); $S_3(a_1) = \theta_{324}$ (H$_2$O scissor); $S_4(b_1) = \gamma_{1234}$ (H$_2$O wag); $S_5(b_2) = 2^{-1/2}(r_{23} - r_{24})$ (H$_2$O antisymmetric stretch); $S_6(b_2) = 2^{-1/2}(\theta_{123} - \theta_{124})$ (H$_2$O rock); $S_7(a_1) = r_{15}$ (Ar−V stretch); $S_8(b_1) = 2^{-1/2}(\alpha^x_{3215} + \alpha^x_{4215})$ (Ar−V−O linear bend in xz plane); and $S_9(b_2) = 2^{-1/2}(\alpha^y_{3215} + \alpha^y_{4215})$ (Ar−V−O linear bend in yz plane), where r_{ij} denotes the bond distance between atoms i and j, θ_{ijk} is the i-j-k bond angle, γ_{ijkl} is the out-of-plane angle of the ij bond with respect to the j-k-l plane, and α^x_{ijkl} and α^y_{ijkl} are linear bends[76] of the jkl chain perpendicular to (α^x) or within (α^y) the ijk plane. The full quartic (quadratic) force fields for V$^+$(H$_2$O) and ArV$^+$(H$_2$O) were computed via 183 (17) and 568 (30) energies points, respectively. The step size for displacements was 0.01 Å and 0.02 rad for bond lengths and angles, respectively. Great effort was made to ensure continuity of both Hartree−Fock and coupled-cluster solutions by slow incremental variations from equilibrium when the species were distorted from C_{2v} symmetry. The program INTDIF2005[77,78] was employed to determine the required displacements as well as compute the force constants in internal coordinates. The transformation of the force constants from internal to normal coordinates and the computation of spectroscopic constants were performed using the programs INTDER2005[79–82] and ANHARM,[82,83] respectively.

All electronic structure computations were performed using the ACES II[84] and MOLPRO[85] suites of programs. Most of the computations were nonrelativistic; however, final energetic predictions for the V$^+$(H$_2$O) ground state were scrutinized by including the one-electron mass−velocity and Darwin scalar relativistic terms[86–90] via the first-order perturbation scheme implemented in ACES II.

III. Results and Discussion

A. V$^+$(H$_2$O) Complex. For the vanadium cation, the lowest-lying quintet state ^5D arises from the 3d^4 configuration and the

TABLE 2: Adiabatic Excitation Energies T_e (T_0) in kcal mol^{-1} within the Lowest-Lying Electronic Manifold^a of V$^+$(H$_2$O) and ArV$^+$(H$_2$O)

V$^+$(H$_2$O)	$^5A_1$	$^5A_2$	$^5B_1$	$^5B_2$
	present work			
ROHF/Wf(TZP)	0	0.02 (0.03)	4.30	6.44
CCSD/Wf(TZP)	0	0.19 (0.20)	0.75	4.99
CCSD(T)/Wf(TZP)	0	0.14 (0.16)	0.67	5.45
ROHF/QZVPP	0	0.02 (0.02)	4.27	6.40
CCSD/QZVPP	0	0.25 (0.27)	0.47	4.57
CCSD(T)/QZVPP	0	0.15 (0.16)	0.37	5.09
	previous theory			
MCPF/Wachters+f TZP^b	0	0.09	6.0	1.5
MP2/6-311++G**^{c}	0	0.07		
CCSD(T)/6-311++G**//	0	0.21		
MP2/6-311++G**^{c}				
B3LYP/B3//B3LYP/B2^{d,e}	0	(0.5)	(0.2)	(4.7)

ArV$^+$(H$_2$O)	$^5A_1$	$^5A_2$	$^5B_1$	$^5B_2$
	present work			
ROHF/ Wf(TZP)	0	0.02	4.35	6.52
CCSD/ Wf(TZP)	0	0.15	0.01	4.10
CCSD(T)/Wf(TZP)	0.40	0.53	0	4.25
ROHF/QZVPP (min 1)	0	0.02	4.22	6.52
ROHF/QZVPP (min 2)	0	0.04	4.37	7.19
CCSD/QZVPP	0.10	0.27	0	3.98
CCSD(T)/QZVPP	0.49	0.62	0	4.17

^{a} A second, higher-lying $^5A_1$ state arising from the five-fold degenerate V$^+$(^5D) atomic state was not examined in detail here. See text. ^{b} References 40 and 41. ^{c} Reference 43. ^{d} Reference 45. ^{e} See footnote e of Table 1 for basis explanation.

first excited state is ^5F (3d^{3}4s). The $^5D_0 \rightarrow ^5F_1$ excitation energy between the lowest-lying spin−orbit sublevels in these manifolds is 2604.82 cm^{-1}.[91] Applying our single-reference electronic structure methods (without spin−orbit coupling) in C_{2v} symmetry to atomic V$^+$(^5D), we find a four-fold degeneracy for the lowest energy solution, with the fifth component (3d$^1_{xy}$3d$^1_{yz}$3d$^1_{xz}$3d$^1_{x^2-y^2}$) very slightly higher in energy. The degeneracy splitting is 0.17 kcal mol^{-1} for ROHF/Wf(TZP), but an utterly negligible 0.00055 kcal mol^{-1} for CCSD(T)/Wf(TZP). We conclude that artifactual degeneracy splitting within the V$^+$(^5D) manifold is not a concern here and that the CCSD(T) method is sufficient to effectively restore the five-fold degeneracy that must be present in the full CI limit.

Complexation with water genuinely splits the five degenerate components of the V$^+$ ground state and in C_{2v} symmetry (Figure 1) gives rise to two $^5A_1$ states, as well as $^5A_2$, $^5B_1$, and $^5B_2$ states. The V$^+$ atomic configurations to which these states asymptotically correlate are $^5A_1$(3d$^1_{xy}$3d$^1_{yz}$3d$^1_{xz}$3d$^1_{z^2}$), $^5A_1$(3d$^1_{xy}$3d$^1_{yz}$3d$^1_{xz}$3d$^1_{x^2-y^2}$), $^5A_2$(3d$^1_{x^2-y^2}$3d$^1_{yz}$3d$^1_{xz}$3d$^1_{z^2}$), $^5B_1$(3d$^1_{xz}$3d$^1_{x^2-y^2}$3d$^1_{xy}$3d$^1_{z^2}$), and $^5B_2$(3d$^1_{xz}$3d$^1_{x^2-y^2}$3d$^1_{xy}$3d$^1_{z^2}$), assuming the axis convention in Figure 1. Because the open-shell vanadium d orbitals retain their atomic character in the electrostatic V$^+$(H$_2$O) and ArV$^+$(H$_2$O) complexes, there is little mixing of the two low-lying $^5A_1$ states. In particular, (12 e$^-$/13 MO) state-specific CASSCF computations on V$^+$(H$_2$O) with the Wf(TZP) basis set gave leading CI coefficients in the natural orbital basis of (0.9780, −0.0769) and (0.0769, 0.9780) for the two $^5A_1$ states, with no other coefficients larger than 0.06. In this work, only the lowest $^5A_1$ state will be fully examined, because we are mostly interested in the ground state for this system and because standard coupled-cluster methods are susceptible to variational collapse if applied to the upper $^5A_1$ state.

Relative energies, optimum geometries, dissociation energies, and vibrational frequencies for the four lowest-lying states of V$^+$(H$_2$O) are presented in Tables 1−4. All four states are within

TABLE 3: Optimum Geometric Parameters (Å, degree) for the Lowest-Lying $^5A_1$, $^5A_2$, $^5B_1$, and $^5B_2$ States of V$^+$(H$_2$O) and for Free Water

		r(V−O)	r(O−H)	θ(H−O−H)
$^5A_1$	ROHF/Wf(TZP)	2.1481	0.9513	107.41
	CCSD/Wf(TZP)	2.0878	0.9699	106.93
	CCSD(T)/Wf(TZP)	2.0774	0.9720	106.93
	ROHF/QZVPP	2.1427	0.9465	107.46
	CCSD/QZVPP	2.0626	0.9601	106.73
	CCSD(T)/QZVPP	2.0492	0.9629	106.76
	MCPF/Wachters+f TZP[a]	2.091		
	MP2/6-311++G**[b]	2.069	0.965	106.9
	B3LYP/DZVP[c]	2.109	0.971	107.4
	B3LYP/B3//3LYP/B2[d]	2.086		
	B3LYP TZVP+G(3df,2p)[e]	2.10	0.966	107.8
$^5A_2$	ROHF/Wf(TZP)	2.1484	0.9513	107.40
	CCSD/Wf(TZP)	2.0876	0.9699	106.81
	CCSD(T)/Wf(TZP)	2.0783	0.9719	106.83
	ROHF/QZVPP	2.1430	0.9465	107.45
	CCSD/QZVPP	2.0611	0.9602	106.58
	CCSD(T)/QZVPP	2.0509	0.9628	106.63
	MCPF/Wachters+f TZP[a]	2.093		
	B3LYP/B3//3LYP/B2[d]	2.084		
$^5B_1$	ROHF/Wf(TZP)	2.1810	0.9520	107.23
	CCSD/Wf(TZP)	2.0670	0.9707	107.01
	CCSD(T)/Wf(TZP)	2.0430	0.9729	107.23
	ROHF/QZVPP	2.1725	0.9472	107.30
	CCSD/QZVPP	2.0449	0.9609	106.75
	CCSD(T)/QZVPP	2.0193	0.9637	107.05
	MCPF/ Wachters+f TZP[a]	2.051		
	B3LYP/B3//3LYP/B2[d]	2.056		
$^5B_2$	ROHF/Wf(TZP)	2.2425	0.9516	106.77
	CCSD/Wf(TZP)	2.1276	0.9697	106.28
	CCSD(T)/Wf(TZP)	2.0965	0.9719	106.49
	ROHF/QZVPP	2.2320	0.9469	106.86
	CCSD/QZVPP	2.1005	0.9601	106.03
	CCSD(T)/QZVPP	2.0672	0.9627	106.31
	MCPF/ Wachters+f TZP[a]	2.117		
	B3LYP/B3//3LYP/B2[d]	2.124		
H$_2$O	RHF/TZP[f]		0.9441	106.41
	CCSD/TZP		0.9652	104.27
	CCSD(T)/TZP		0.9673	104.02
	RHF/aug-cc-pVQZ[f]		0.9398	106.33
	CCSD/aug-cc-pVQZ		0.9561	104.62
	CCSD(T)/aug-cc-pVQZ		0.9590	104.37
	Exact, empirical[g]		0.9578	104.48

[a] References 40 and 41. [b] Reference 43. [c] Reference 44. [d] Reference 45. [e] Reference 38. [f] TZP and aug-cc-pVQZ basis sets for free H$_2$O respectively correspond to the Wf(TZP) and QZVPP basis sets for V$^+$(H$_2$O). [g] References 94−96.

6 kcal mol^{-1} of one another. The ground state is the $^5A_1$ state for all applied levels of theory. The electronic configuration for the singly occupied orbitals of the ground state in C_{2v} symmetry is $1a_2 4b_2 4b_1 9a_1$, which agrees with previous results.[40,41,43] All of these molecular orbitals correspond to atomic orbitals on vanadium: $1a_2$ to $3d_{xy}$, $4b_2$ to $3d_{yz}$, $4b_1$ to $3d_{xz}$, and $9a_1$ to a mixture of the $3d_{z^2}$ and $4s$ orbitals, as mentioned by Rosi and Bauschlicher.[40,41] The fascinating hybrid character of the $9a_1$ orbital is illustrated in Figure 2.

The V−O distance, O−H distance, and H−O−H angle for the ground state of V$^+$(H$_2$O) are 2.049 Å, 0.963 Å, and 106.8°, respectively, at the CCSD(T)/QZVPP level of theory (Table 3). The H−O−H angle computed at the same level of theory for free water is 104.4°, which is 2.4° less than that of the V$^+$(H$_2$O) complex. The H−O−H angle expansion resulting from the addition of the vanadium cation is much smaller than the aforementioned IRPD spectroscopic result (9.3°) of Duncan et al.[21] The complexation effect on the H−O−H angle is not particularly sensitive to the level of theory; indeed, among the six sets of optimum geometries we computed in this study (Table

3), the angle widening lies in the range 1.0−2.9°. The predicted H−O−H angle for V$^+$(H$_2$O) is even less sensitive to the computational method than for the corresponding angle in free water. For V$^+$(H$_2$O), the change in the H−O−H angle due to basis set and electron correlation improvements [ROHF/Wf(TZP) to CCSD(T)/QZVPP] only approaches 0.8° for the $^5A_1$ and $^5A_2$ states of V$^+$(H$_2$O) and is only 0.2° for the $^5B_1$ state of V$^+$(H$_2$O). By comparison, the angle for free water computed with CCSD(T)/QZVPP (104.4°) is 2.0° smaller than that computed with ROHF/Wf(TZP) (106.4°).

Moving an electron in V$^+$(H$_2$O) from the $1a_2$ ($3d_{xy}$) to the $10a_1$ ($3d_{x^2-y^2}$) orbital results in a $^5A_2$ state that is almost degenerate with the ground state, as the energy difference is only 0.15 kcal mol^{-1} for the CCSD(T)/QZVPP level of theory (Table 2). The $T_e(^5A_2)$ excitation energy is not very sensitive to electron correlation or basis set, varying by only 0.1−0.2 kcal mol^{-1} in Table 2. Our $^5A_2 - {}^5A_1$ separation of 0.15 kcal mol^{-1} generally validates the relative energies of 0.09 kcal mol^{-1} obtained by Rosi and Bauschlicher,[40,41] and 0.07 kcal mol^{-1} obtained by Trachtman et al.[43] The geometry difference between the $^5A_2$ state and the $^5A_1$ ground state is also very small. The V−O bond distance for the $^5A_2$ state is only 0.002 Å longer than the corresponding distance for the $^5A_1$ state [CCSD(T)/ QZVPP]. The H−O−H angle for the $^5A_2$ state differs from the $^5A_1$ ground state value by less than 0.1° [CCSD(T)/QZVPP].

The $^5B_1$ and $^5B_2$ states of V$^+$(H$_2$O) are 0.4 and 5.1 kcal mol^{-1} [CCSD(T)/QZVPP], respectively, above the ground state. Electron correlation lowers both states substantially, by almost 4 kcal mol^{-1} for the $^5B_1$ state, making ($^5A_1$, $^5A_2$, $^5B_1$) isoenergetic within 0.5 kcal mol^{-1}. The trend with increasing basis set is a further lowering of the $^5B_1$ and $^5B_2$ excited states. The B3LYP results of Klippenstein and Yang[45] also give a ($^5A_1$, $^5A_2$, $^5B_1$) cluster of states within 0.5 kcal mol^{-1}, but the ($^5A_2$, $^5B_1$) ordering is switched with respect to our high-level CCSD(T)/QZVPP predictions. The ordering of $^5B_1$ and $^5B_2$ states reported by Rosi and Bauschlicher[40,41] (T_e = 6.0 kcal mol^{-1} for $^5B_1$ and 1.5 kcal mol^{-1} for $^5B_2$) is reversed compared to our best results. This disparity might merely be a labeling issue for the C_{2v} irreducible representations, although their axis conventions appear to be the same as ours. The CCSD(T)/QZVPP method yields optimum H−O−H angles for the $^5B_1$ and $^5B_2$ states that are respectively 0.29° above and 0.45° below the corresponding ground state value of 106.76°. Finally, the $^5B_1$ state exhibits the shortest equilibrium V−O bond distance [2.019 Å, CCSD(T)/QZVPP] among the four lowest-lying electronic states. The sequence of V−O bond distances (but not relative energies) for these states can be simplistically rationalized by hypothesizing that single occupation of the vanadium 3d orbitals hinders charge donation to the metal-cation center in the rough ordering $d_{xy}, d_{yz} < d_{x^2-y^2} < d_{xz}, d_{z^2}$, in accord with the symmetries and density profiles of the oxygen lone pair orbitals.

Correlation of the 3s3p shell on vanadium is important for the evaluation of the excitation energies. The QZVPP basis was explicitly constructed to allow polarization of the 3s3p shell, and it has been recommended that this shell be included in correlation treatments with this basis set of the 3d series of transition metals.[68] We performed CCSD(T)/QZVPP single-point energy computations with V(3s) and V(3p) frozen to see what changes in excitation energies would be engendered. The corresponding small-core optimum geometries were employed. The resulting excitation energies were 0.15 kcal mol^{-1}, 0.88 kcal mol^{-1}, and 4.95 kcal mol^{-1} for the $^5A_2$, $^5B_1$, and $^5B_2$ states, respectively. Thus, the ordering of the states of V$^+$(H$_2$O) is preserved if the frozen core is expanded, but the excitation

V$^+$(H$_2$O) and ArV$^+$(H$_2$O) Complexes

J. Phys. Chem. A, Vol. 111, No. 31, 2007 **7603**

TABLE 4: Harmonic Vibrational Frequencies (in cm^{-1}) for the Four Lowest-Lying States of V$^+$(H$_2$O) and for Free Water

		$\omega_1(a_1)$	$\omega_2(a_1)$	$\omega_3(a_1)$	$\omega_4(b_1)$	$\omega_5(b_2)$	$\omega_6(b_2)$
		O−H sym stretch	H$_2$O scissor	V−O stretch	H$_2$O wag	O−H asym stretch	H$_2$O rock
$^5A_1$	ROHF/Wf(TZP)	4036	1794	364	385	4116	568
	CCSD/Wf(TZP)	3795	1679	407	266	3879	553
	CCSD(T)/Wf(TZP)	3763	1666	419	232	3849	554
	ROHF/QZVPP	4041	1792	368	370	4117	561
	CCSD/QZVPP	3836	1692	428	330	3916	524
	CCSD(T)/QZVPP	3794	1675	449	304	3876	527
$^5A_2$	ROHF/Wf(TZP)	4037	1795	364	386	4116	568
	CCSD/Wf(TZP)	3795	1682	408	265	3878	557
	CCSD(T)/Wf(TZP)	3764	1669	417	235	3849	557
	ROHF/QZVPP	4041	1793	367	371	4117	562
	CCSD/QZVPP	3836	1696	432	328	3915	532
	CCSD(T)/QZVPP	3795	1679	443	306	3877	531
$^5B_1$	ROHF/Wf(TZP)	4026	1789	312	^{a}	^{a}	^{a}
	CCSD/Wf(TZP)	3784	1675	396	^{a}	^{a}	^{a}
	CCSD(T)/Wf(TZP)	3750	1660	426	^{a}	^{a}	^{a}
	ROHF/QZVPP	4030	1786	316	^{a}	^{a}	^{a}
	CCSD/QZVPP	3826	1689	416	^{a}	^{a}	^{a}
	CCSD(T)/QZVPP	3782	1671	451	^{a}	^{a}	^{a}
$^5B_2$	ROHF/Wf(TZP)	4033	1789	291	^{a}	^{a}	^{a}
	CCSD/Wf(TZP)	3801	1677	365	^{a}	^{a}	^{a}
	CCSD(T)/Wf(TZP)	3768	1663	402	^{a}	^{a}	^{a}
	ROHF/QZVPP	4036	1786	295	^{a}	^{a}	^{a}
	CCSD/QZVPP	3841	1690	387	^{a}	^{a}	^{a}
	CCSD(T)/QZVPP	3800	1673	432	^{a}	^{a}	^{a}
H$_2$O	RHF/TZP^b	4122	1736			4230	
	CCSD/TZP	3832	1639			3943	
	CCSD(T)/TZP	3800	1629			3913	
	RHF/aug-cc-pVQZ^b	4128	1747			4229	
	CCSD/aug-cc-pVQZ	3874	1663			3981	
	CCSD(T)/aug-cc-pVQZ	3831	1649			3940	
	experiment^{c,d}	3832.2	1648.5			3942.5	

^{a} Upon distortion along b_1 or b_2 normal modes, $^5B_1$ and $^5B_2$ are no longer the lowest quintet states of the irreps (A' or A'') in C_s symmetry to which they correlate. Therefore, variational collapse of the excited-state $^5B_1$ and $^5B_2$ solutions is a concern for the electronic structure methods applied here, all based on a Hartree−Fock reference wave function. Accordingly, $\omega_4-\omega_6$ for the $^5B_1$ and $^5B_2$ states are suspect and were not computed. ^{b} TZP and aug-cc-pVQZ basis sets for free H$_2$O respectively correspond to the Wf(TZP) and QZVPP basis sets for V$^+$(H$_2$O) ^{c} References 94−96. ^{d} CVRQD potential energy surface of refs 99 and 100 provides the best ab initio harmonic vibrational frequencies of water to date: $\omega_1 = 3833.0$ cm^{-1}, $\omega_2 = 1648.8$ cm^{-1}, and $\omega_3 = 3944.1$ cm^{-1}. Adjusted for the small deviations of the CVRQD fundamental frequencies from experiment, one obtains $\omega_1 = 3833.7$ cm^{-1}, $\omega_2 = 1648.5$ cm^{-1}, and $\omega_3 = 3945.1$ cm^{-1} as perhaps the best current values for the harmonic frequencies of water.
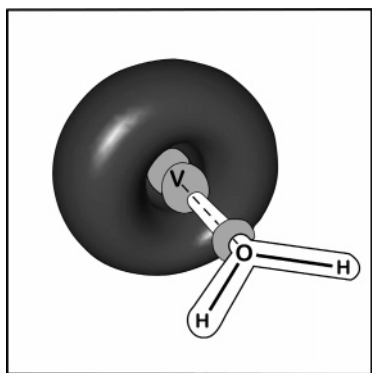

Figure 2. HOMO of the V$^+$(H$_2$O) $^5A_1$ ground state. The two different shades indicate the sign of the orbital lobes.

energies change for the $^5B_1$ and $^5B_2$ states by $+0.51$ kcal mol^{-1} and -0.14 kcal mol^{-1}, respectively (cf. Table 2).

In our optimum geometric structures, the V−O distance decreases substantially with improvements in both the basis set and the electron correlation treatment. However, this occurrence is typical of electrostatically bound complexes between polarizable species. Note that, for the $^5B_1$ and $^5B_2$ states of V$^+$(H$_2$O), the contraction of the V−O distance from ROHF/Wf(TZP) to CCSD(T)/QZVPP approaches 0.2 Å. Our best [CCSD(T)/QZVPP] predictions for r(V−O) are as much as 0.05 Å shorter

than previous theoretical values but are probably still upper bounds on the exact equilibrium distance.

The lowest-lying triplet electronic state ($^3B_2$) of V$^+$(H$_2$O) reported by Rosi and Bauchslicher[40,41] lies 22 kcal mol^{-1} higher in energy than the quintet ground state (MCPF/Wachters+f TZP). Irigoras et al.[44] found the lowest triplet state to be $^3A_1$, lying 18.1 kcal mol^{-1} above the $^5A_1$ state [B3LYP/TZVP+G-(3df,2p)]. We performed CCSD(T)/Wf(TZP) single-point energy computations for various triplet electronic states at the V$^+$(H$_2$O) $^5A_1$ CCSD(T)/Wf(TZP) geometry. We found the lowest triplet state of V$^+$(H$_2$O) to be $^3B_2$ with a vertical excitation energy of 19.6 kcal mol^{-1}. In summary, the triplet states of V$^+$(H$_2$O) are sufficiently higher in energy than the low-lying quintet manifold to be excluded from further consideration in this work.

The ZPVE corrected dissociation energy (D_0) of the V$^+$(H$_2$O) ground state, corresponding to dissociation into V$^+$(^5D) + H$_2$O, is computed to be 36.2 kcal mol^{-1} at our best level of theory [CCSD(T)/QZVPP]. The basis set and electron correlation trends in Table 1 suggest that our D_0 value is converged to within 1 kcal mol^{-1}. Indeed, our (nonrelativistic) dissociation energy of 36.2 ± 1.0 kcal mol^{-1} is within the error bars of all experimental studies (Table 1) and provides the most accurate dissociation energy of the V$^+$(H$_2$O) complex to date. Among the theoretical studies on D_e(V$^+$−H$_2$O), the 6-311++G** CCSD(T) dissociation energy reported in ref 43 is unusually large ($\Delta H^{\circ}_{298} = 41.8$ kcal mol^{-1} for the bond enthalpy and $D_e = 43.4$ kcal

7604 *J. Phys. Chem. A, Vol. 111, No. 31, 2007*

Kasalová et al.

mol^{-1}). We performed single-point CCSD(T)/6-311++G** energy computations at the CCSD(T)/QZVPP optimized geometry and found that the dissociation energy D_e for production of V$^+$(^5D) is 34.0 kcal mol^{-1}, while dissociation into V$^+$(^5F) requires 41.3 kcal mol^{-1} of energy. For this reason, we conclude that the CCSD(T) dissociation energy reported in ref 43 likely corresponds to an incorrect dissociation asymptote.

The effects of core correlation and special relativity on the binding energy of V$^+$(H$_2$O) warrant consideration. If the 3s and 3p outer-core orbitals on vanadium are not correlated, against the recommendation of Weigend et al.,[68] the V$^+$−H$_2$O dissociation energy decreases by almost 5 kcal mol^{-1} at our best level of theory [CCSD(T)/QZVPP]. When ZPVE is added, the dissociation energy becomes $D_0 \sim$ 31.4 kcal mol^{-1}, an anomalously small value compared to experimental measurements. Clearly, correlation treatments with large frozen cores are not advisable for this system, at least with the QZVPP basis. With regard to relativistic corrections, the one-electron mass−velocity and Darwin terms shift the dissociation energy of the V$^+$(H$_2$O) $^5A_1$ ground state by +0.48 kcal mol^{-1} at the CCSD(T)/QZVPP level, that is, well within our stated error bars. To further pinpoint the various auxiliary effects on D_0(V$^+$−H$_2$O) would require multicomponent relativistic treatments and an accounting of shifts in the atomic V$^+$ spin−orbit splittings engendered by H$_2$O complexation.

The harmonic vibrational frequencies of the four lowest-lying states of V$^+$(H$_2$O) are listed with associated results for free water in Table 4. At the highest level of theory [CCSD(T)/QZVPP], analogous frequencies of the four electronic states of V$^+$(H$_2$O) never differ by more than 20 cm^{-1}, and for the $^5A_1$ and $^5A_2$ states, the ω_i values are almost identical. It is thus sufficient to focus our discussion on the ground-state $^5A_1$ frequencies.

First note in Table 4 that CCSD(T) theory with the aug-cc-pVQZ basis reproduces the empirical harmonic frequencies of H$_2$O to exceptional accuracy (within 2 cm^{-1} in every case). Because the QZVPP set for V$^+$(H$_2$O) contains the aug-cc-pVQZ basis on the H$_2$O moiety, we expect the frequencies of the H$_2$O modes to be very accurately predicted with the CCSD(T)/QZVPP method. The O−H symmetric and antisymmetric harmonic stretching frequencies of $^5A_1$ V$^+$(H$_2$O) are ω_1 = 3794 cm^{-1} and ω_5 = 3876 cm^{-1} [CCSD(T)/QZVPP], representing red shifts of 37 cm^{-1} and 64 cm^{-1}, respectively, from free water. Among the correlated electronic structure methods in Table 4, there is striking agreement (within 1 cm^{-1}) on the magnitude of these red shifts, enhancing the credence of the predictions. As shown in Table 8, vibrational anharmonicity increases the red shifts of the symmetric and antisymmetric O−H stretches to 43 cm^{-1} and 72 cm^{-1}, respectively. These theoretical results nicely substantiate the red shifts of ∼50 cm^{-1} and ∼70 cm^{-1} observed by Duncan's group.[21] This general agreement is maintained when the effects of argon tagging are considered in the next section (IIIB), despite some subtle changes brought on by the Ar "spectator".

The H$_2$O harmonic scissoring frequency of $^5A_1$ V$^+$(H$_2$O) is ω_2 = 1675 cm^{-1} [CCSD(T)/QZVPP], constituting a blue shift of 26 cm^{-1} relative to free water. Vibrational anharmonicity has no discernible effect on this complexation shift (Table 8). It is remarkable that a blue shift occurs in the scissoring frequency simultaneously with H−O−H angle widening (2−3°) and O−H bond elongation (∼0.004 Å). A simple explanation of the ω_2 blue shift is that the inherent barrier to linearity of water is increased by the presence of the vanadium cation, because the bent, equilibrium structure of H$_2$O has a large dipole moment ($\mu \approx$ 1.85 D) to enhance electrostatic
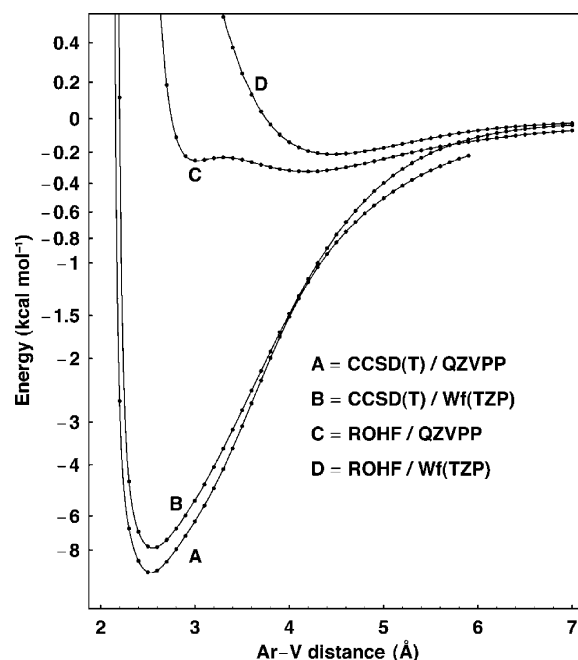

Figure 3. Theoretical argon dissociation curves for the $^5A_1$ state of ArV$^+$(H$_2$O). In this plot, V$^+$(H$_2$O) is fixed at its optimum structure for the corresponding level of theory; only the Ar−V distance was changed. Note the nonuniform scale on the energy axis, which is necessary to reveal the shallow ROHF minima.

binding, whereas the linear structure of H$_2$O (with μ = 0) is devoid of this strong, first-order interaction. Accordingly, the bent structure of H$_2$O would lie in a deeper well of the bending potential and thus exhibit a larger quadratic scissoring force constant upon complexation, as seen by comparing data in Tables S2 and S4 of Supporting Information.

The harmonic frequencies for the interfragment modes of V$^+$(H$_2$O) occur in the 300−550 cm^{-1} range. Perhaps the most noteworthy trend for these modes is the increase in the V−O stretching frequency with improvements in both the basis set and the electron correlation treatment, in accord with the bond length contractions observed in Table 3. Our best prediction [CCSD(T)/QZVPP] for the V−O stretching frequency of $^5A_1$ V$^+$(H$_2$O) is ω_3 = 449 cm^{-1} or ν_3 = 438 cm^{-1} if vibrational anharmonicity is included (Table 8). Consistent with this theoretical result, Lessen and co-workers[1] report a V−O stretch of ω_e'' = 420 ± 75 cm^{-1} from a resonant one-photon fragmentation spectrum of V$^+$(H$_2$O).

B. ArV$^+$(H$_2$O) Complex. Similarly to V$^+$(H$_2$O), the four lowest-lying quintet electronic states were investigated for the ArV$^+$(H$_2$O) complex. Relative energies, geometries, dissociation energies, and harmonic vibrational frequencies for the $^5A_1$, $^5A_2$, $^5B_1$, and $^5B_2$ states are listed in Tables 2 and 5−7. Fundamental vibrational frequencies and anharmonicities of ArV$^+$(H$_2$O), V$^+$(H$_2$O), and free H$_2$O are compared in Table 8.

As in the V$^+$(H$_2$O) case, the triplet electronic states are sufficiently high in energy to be excluded from detailed consideration here. Specifically, CCSD(T)/Wf(TZP) single-point energy computations on the triplet electronic states of ArV$^+$(H$_2$O) at the $^5A_1$ CCSD(T)/Wf(TZP) optimized geometry gave two $^3B_2$ and two $^3B_1$ states in a range of 29.0 to 33.3 kcal mol^{-1}. Therefore, triplet electronic states of ArV$^+$(H$_2$O) were not considered further.

The dissociation energy profile with respect to the Ar−V distance of ArV$^+$(H$_2$O) for various levels of theory is presented in Figure 3. The striking feature of Figure 3 is that significant binding of Ar to V$^+$(H$_2$O) is obtained only with correlated wave

TABLE 5: Optimum Geometric Parameters (Å, degree) for the Lowest-Lying $^5A_1$, $^5A_2$, $^5B_1$, and $^5B_2$ States of ArV$^+$(H$_2$O)^a

		r(Ar–V)	r(V–O)	r(O–H)	θ(H–O–H)
$^5A_1$	ROHF/Wf(TZP)	4.4685	2.1477	0.9513	107.43
	CCSD/Wf(TZP)	2.5666	2.1056	0.9691	106.71
	CCSD(T)/Wf(TZP)	2.5503	2.1004	0.9712	106.64
	ROHF/QZVPP (min 1)	3.0198	2.1378	0.9457	107.61
	ROHF/QZVPP (min 2)	4.1857	2.1421	0.9464	107.49
	CCSD/QZVPP	2.5553	2.0762	0.9595	106.44
	CCSD(T)/QZVPP	2.5298	2.0698	0.9622	106.37
$^5A_2$	ROHF/Wf(TZP)	4.4740	2.1481	0.9512	107.41
	CCSD/Wf(TZP)	2.5641	2.1065	0.9691	106.60
	CCSD(T)/Wf(TZP)	2.5486	2.1014	0.9711	106.55
	ROHF/QZVPP (min 1)	3.0298	2.1382	0.9457	107.58
	ROHF/QZVPP (min 2)	4.1968	2.1424	0.9464	107.48
	CCSD/QZVPP	2.5520	2.0768	0.9595	106.32
	CCSD(T)/QZVPP	2.5279	2.0707	0.9622	106.27
$^5B_1$	ROHF/Wf(TZP)	4.7529	2.1800	0.9520	107.25
	ROHF/Wf(TZP)	2.5627	2.0736	0.9701	106.89
	CCSD(T)/Wf(TZP)	2.5492	2.0654	0.9722	106.87
	ROHF/QZVPP (min 1)	2.7897	2.1325	0.9453	107.60
	ROHF/QZVPP (min 2)	4.6273	2.1708	0.9472	107.34
	CCSD/QZVPP	2.5594	2.0482	0.9604	106.62
	CCSD(T)/QZVPP	2.5376	2.0387	0.9632	106.62
$^5B_2$	ROHF/Wf(TZP)	4.8743	2.2423	0.9516	106.78
	CCSD/Wf(TZP)	2.5606	2.1358	0.9692	106.26
	CCSD(T)/Wf(TZP)	2.5472	2.1283	0.9713	106.24
	ROHF/QZVPP (min 1)	2.7748	2.1902	0.9449	106.94
	ROHF/QZVPP (min 2)	4.7948	2.2316	0.9468	106.87
	CCSD/QZVPP	2.5564	2.1041	0.9597	106.00
	CCSD(T)/QZVPP	2.5345	2.0956	0.9624	105.99

^{a} A second, higher-lying $^5A_1$ state arising from the five-fold degenerate V$^+$(^5D) atomic state was not examined in detail here. See text.

TABLE 6: Argon Binding Energies^a [$D_e(D_0)$ in kcal mol^{-1}] for the $^5A_1$ and $^5B_1$ States of ArV$^+$(H$_2$O)

	$^5A_1$	$^5B_1$
ROHF/Wf(TZP)	0.21(0.17)	−4.14
CCSD/Wf(TZP)	6.89(6.46)	6.87
CCSD(T)/Wf(TZP)	7.91	8.31
ROHF/QZVPP	0.25	−3.97
CCSD/QZVPP	8.01	8.12
CCSD(T)/QZVPP	9.42	9.91 (9.36)^b

^{a} All values are referenced to the ground-state $^5A_1$ V$^+$(H$_2$O) + Ar fragments. ^{b} Computation of the ZPV effect on the argon binding energy is complicated by difficulties in determining the CCSD(T)/QZVPP b_1 vibrational frequencies of $^5B_1$ ArV$^+$(H$_2$O). Here, we assumed that the H$_2$O wagging frequency does not change with Ar tagging and the Ar–V–O out-of-plane linear bend has the same frequency (84 cm^{-1}) as the corresponding in-plane linear bend. This approach provides a reasonable accounting of ZPVE within ca. 0.1 kcal mol^{-1} in the presence of intricate vibronic coupling within the ($^5A_1$, $^5B_1$, $^5A_2$) manifold.

functions, even though the basic nature of the attraction is "electrostatic". While Figure 3 explicitly shows only the $^5A_1$ potential curves, the curves for the other states are nearly identical. At the ROHF/Wf(TZP) level, the equilibrium Ar–V bond is extremely large (>4 Å) for all four states. With ROHF/QZVPP there is a double minimum for all four studied states of ArV$^+$(H$_2$O). Geometrical structures are reported for both minima in Table 5, and the one with the shorter Ar–V distance is consistently designated min 1. In Tables 2 and 6, relative energies and dissociation energies are reported for the lower-energy minimum only (min 1 for $^5B_1$; min 2 for $^5A_1$, $^5A_2$, and $^5B_2$). Minima designated as min 2 are no longer present when correlation is introduced at the CCSD or CCSD(T) level.

When argon is added to the V$^+$(H$_2$O) complex, the ordering of the lowest-lying states changes, even though Ar would generally be considered a spectator atom. At the ROHF level of theory, no reordering of states is seen due to the large Ar–V distance; the $^5A_1$ state is the lowest energetically (Table 2). However, the $^5B_1$ state is predicted to be the ground electronic state of ArV$^+$(H$_2$O) for correlated methods, except in the CCSD/Wf(TZP) case, where $^5A_1$ is a mere 0.01 kcal mol^{-1} below $^5B_1$. Our best level of theory [CCSD(T)/QZVPP] gives a $^5A_1 - ^5B_1$ separation of $T_e = 0.49$ kcal mol^{-1}, and the $^5A_2$ state is predicted to be only slightly higher ($T_e = 0.62$ kcal mol^{-1}).

The CCSD(T)/QZVPP argon–vanadium distance for the $^5B_1$ ground state (2.538 Å) differs by less than 0.01 Å from the corresponding distances for the other three states (Table 5). In general, the Ar–V distance for all four states gets smaller as correlation is added to the system. The CCSD(T)/QZVPP vanadium–oxygen distance varies from 2.039 Å ($^5B_1$) to 2.096 Å ($^5B_2$); the O–H distance is predicted to be 0.963 Å for the ground state and 0.962 Å for the $^5A_1$, $^5A_2$, and $^5B_2$ states; and the H–O–H angle ranges from 105.99° ($^5B_2$) to 106.62° ($^5B_1$). The r(V–O) contraction in ArV$^+$(H$_2$O) with improvements in both the basis set and the treatment of electron correlation is

not as large as in the untagged ion. The contraction of the V–O distance from ROHF/Wf(TZP) to CCSD(T)/QZVPP is between ∼0.08 Å ($^5A_1$, $^5A_2$) and ∼0.14 Å ($^5B_1$, $^5B_2$). Our best CCSD(T)/QZVPP prediction for r(V–O) of the $^5B_1$ ground state is 2.039 Å.

Comparison of data in Tables 3 and 5 reveals the effect of argon tagging in the geometric structure of V$^+$(H$_2$O). Forming the Ar adduct while maintaining the electronic state as $^5A_1$ shifts r(V–O), r(O–H), and θ(H–O–H) by +0.0206 Å, −0.0007 Å, and −0.39°, respectively, at the CCSD(T)/QZVPP level. However, argon addition changes the ground electronic state to $^5B_1$, and if this state switching is considered, the tagging effect [CCSD(T)/QZVPP] on r(V–O), r(O–H), and θ(H–O–H) is −0.0105 Å, +0.0003 Å, and −0.14°, respectively, or roughly half as much. Note that the expected increase in the V–OH$_2$ separation upon argon binding is overcome by the r(V–O) bond length contraction arising from the change of d occupancies when the ground state goes to $^5B_1$ (see section IIIA). In brief, intricacies are encountered upon argon tagging, but the overall structural shifts can certainly be categorized as small perturbations.

Argon binding energies for various levels of theory for both the $^5B_1$ and the $^5A_1$ states of ArV$^+$(H$_2$O) are contained in Table 6. The dissociation energy (D_e) of the ArV$^+$(H$_2$O) $^5B_1$ ground state, corresponding to fragmentation into Ar (^1S) and the $^5A_1$ ground state of V$^+$(H$_2$O), is computed to be 9.9 kcal mol^{-1} at the CCSD(T)/ QZVPP level of theory. While with correlated methods the $^5A_1 - ^5B_1$ separation for ArV$^+$(H$_2$O) is smaller than 0.5 kcal mol^{-1}, at the ROHF level of theory, it is larger than 4 kcal mol^{-1} in favor of the $^5A_1$ state, because of the very weak Ar–V bond (Ar–V equilibrium bond length > 4 Å). This explains the negative ROHF energies for the process $^5B_1$ ArV$^+$(H$_2$O) → Ar(^1S) + $^5A_1$ V$^+$(H$_2$O). The argon binding energy of each of the states of ArV$^+$(H$_2$O) gets larger as the basis set is enlarged and the electron correlation treatment improved, which is consonant with the shrinking Ar–V distance. It is striking that with the Hartree–Fock method the binding energy is less than 1 kcal mol^{-1}, whereas the final D_e from CCSD(T)/QZVPP theory (9.9 kcal mol^{-1}) is quite large. The binding energy of Ar to the V$^+$(H$_2$O) species is comparable to the binding energy measured in the V$^+$Ar diatomic complex (8.76 kcal mol^{-1}).[39]

The ArV$^+$(H$_2$O) complex is further characterized by the harmonic vibrational frequencies in Table 7. The new modes formed by addition of the Ar atom all have frequencies (ω_4, ω_6, ω_9) substantially less than 200 cm^{-1}. The CCSD/Wf(TZP)

TABLE 7: Harmonic Vibrational Frequencies (in cm^{-1}) of the ArV$^+$(H$_2$O) Complex^a

		$\omega_1(a_1)$	$\omega_2(a_1)$	$\omega_3(a_1)$	$\omega_4(a_1)$	$\omega_5(b_1)$	$\omega_6(b_1)$	$\omega_7(b_2)$	$\omega_8(b_2)$	$\omega_9(b_2)$
$^5A_1$	ROHF/Wf(TZP)	4037	1794	364	14	383	8	4117	567	8
$^5A_1$	CCSD/Wf(TZP)	3804	1678	395	163	255	67	3888	542	88
$^5B_1$	CCSD(T)/Wf(TZP)	3759	1662	408	168	655^b	113^b	3845	536	84
$^5A_1$	ROHF/QZVPP	4052	1789	371	34	345	54	4130	548	58
$^5B_1$	CCSD/QZVPP	3833	1688	424	160			3911	506	83
$^5B_1$	CCSD(T)/QZVPP	3790	1671	433	168			3870	606	84

^{a} Results are tabulated for the lowest electronic state at each level of theory. ω_1 = O−H symmetric stretch, ω_2 = H$_2$O scissor, ω_3 = V−O stretch, ω_4 = Ar−V stretch, ω_5 = H$_2$O wag, ω_6 = Ar−V−O out-of-plane linear bend, ω_7 = O−H antisymmetric stretch, ω_8 = H$_2$O rock, ω_9 = Ar−V−O in-plane linear bend. ^{b} The $^5B_1$ state is the lowest one at the CCSD(T) level, but not at the Hartree−Fock level. For b_1 displacements from C_{2v} symmetry, the $^5B_1$ solution for the Hartree−Fock reference wave function can be continuously followed due to the atomic character of the open-shell manifold, but there is no guarantee against variational collapse.
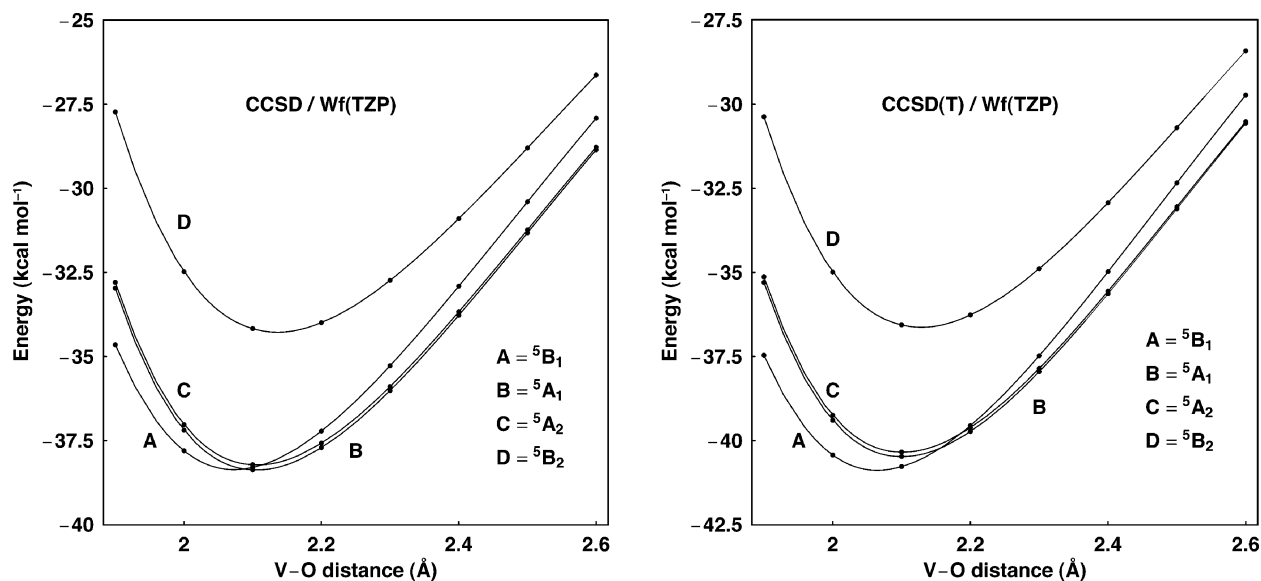

Figure 4. Energy versus the V−O distance of four low-lying states of ArV$^+$(H$_2$O), relative to dissociation into H$_2$O plus the $^5A_1$ state of ArV$^+$, computed at the CCSD and CCSD(T)/Wf(TZP) levels of theory. Constrained optimizations were performed for each plotted V−O distance.

frequencies allow quantification of argon tagging shifts when the $^5A_1$ electronic state is retained. The O−H bond stretches in the H$_2$O moiety are both shifted +9 cm^{-1} in going from $^5A_1$ V$^+$(H$_2$O) to $^5A_1$ ArV$^+$(H$_2$O), with an attendant reduction in the H$_2$O scissoring frequency by less than 2 cm^{-1}. The interfragment V−O stretch, H$_2$O wag, and H$_2$O rock are all reduced in frequency by about 10 cm^{-1}. Vibrational anharmonicity (Table 8) does not appreciably affect any of the argon tagging shifts, provided the $^5A_1$ state is maintained.

The change in the ground state to $^5B_1$ upon argon complexation has some significant consequences, as shown in the CCSD(T)/QZVPP frequencies of V$^+$(H$_2$O) and ArV$^+$(H$_2$O). First, the H$_2$O modes are now all shifted by about −5 cm^{-1} (opposite direction) due to the presence of argon. The interfragment V−O stretch and H$_2$O rock now exhibit larger tagging effects of −16 cm^{-1} and +79 cm^{-1}, respectively. Finally, the H$_2$O wag appears to be strongly influenced by vibronic interactions with the nearby quintic electronic states, as promoted by Ar addition. In fact, we were only able to determine b_1 vibrational frequencies for $^5B_1$ ArV$^+$(H$_2$O) at the CCSD(T)/Wf(TZP) level, because insuperable convergence difficulties were encountered in searching for $^5B_1$ electronic solutions along these modes with the QZVPP basis. This issue is addressed in more detail in the following section (IIIC).

C. Vibrational Anharmonicity Effects. The computation of the nontotally symmetric vibrational frequencies of V$^+$(H$_2$O) and ArV$^+$(H$_2$O) requires extreme care due to the intricate vibronic interactions within the lowest-lying manifold of quintet states precipitated when the equilibrium C_{2v}

symmetry is lowered. Nonetheless, complete vibrational analyses of the $^5A_1$ ground state of V$^+$(H$_2$O) and its $^5A_1$ counterpart in ArV$^+$(H$_2$O) were executed here without severe difficulties. The principal problem we encountered involved the b_1 vibrational modes of the $^5B_1$ state of ArV$^+$(H$_2$O). The $^5B_1$ state is the ground state of ArV$^+$(H$_2$O) at the CCSD(T)/ Wf(TZP), CCSD/QZVPP, and CCSD(T)/QZVPP levels of theory; however, the $^5A_1$ state is lower in energy for the ROHF reference wave function. Because the $^5B_1$ and $^5A_1$ states retain their V$^+$ atomic character in ArV$^+$(H$_2$O), we were able (with much care) to continuously follow the $^5B_1$ ROHF solutions into C_s and C_1 regions where the ($^5B_1$, $^5A_1$) pair is of the same spatial symmetry. Accordingly, a complete and mathematically correct numerical differentiation of the potential energy surface of the $^5B_1$ state of ArV$^+$(H$_2$O) was achieved through quartic terms, despite loss of the variational principle for the b_1 modes.

The resulting CCSD(T)/Wf(TZP) anharmonic force field for $^5B_1$ ArV$^+$(H$_2$O) is given in Supporting Information (Table S1). A number of intriguing cubic and quartic constants are exhibited that are anomalously large in magnitude, all involving the b_1 modes (S_4 and S_8). Many of these anomalous force constants also involve the a_1 V−O stretching coordinate, which appears to exacerbate the problem. The probable origin of this phenomenon is seen in Figure 4, where the potential curves versus r(V−O) for the lowest-lying quintet states of ArV$^+$(H$_2$O) exhibit crossings very near the equilibrium distance. In the full geometric configuration space, conical intersections of the quintet potential energy surfaces are thus present in the vicinity

V$^+$(H$_2$O) and ArV$^+$(H$_2$O) Complexes

J. Phys. Chem. A, Vol. 111, No. 31, 2007 **7607**

TABLE 8: Summary of CCSD/Wf(TZP) VPT2 Anharmonic Vibrational Analysis of the $^5A_1$ States of ArV$^+$(H$_2$O) and V$^+$(H$_2$O)^a

	i	ω_i	Δ_i	ν_i	α_i^A	α_i^B	α_i^C
			ArV$^+$(H$_2$O)				
O−H sym. stretch	1	3804.3	−183.0	3621.3	0.23876	0.0000059	0.0000094
H$_2$O scissor	2	1678.1	−44.0	1634.1	−0.17072	−0.0000060	0.0000086
V−O stretch	3	395.2	−12.8	382.4	−0.00600	0.0002637	0.0002651
Ar−V stretch	4	162.5	−7.5	155.1	0.00181	0.0005642	0.0005542
H$_2$O wag	5	255.4	+124.6	379.9	1.83244	−0.0000202	−0.0000464
Ar−V−O lin. bend (b_1)	6	66.7	+21.7	88.4	0.27989	−0.0000579	−0.0001646
O−H antisym. stretch	7	3888.3	−198.0	3690.3	0.13627	0.0000034	0.0000041
H$_2$O rock	8	542.2	−3.2	539.0	−1.49487	−0.0000101	0.0000116
Ar−V−O lin. bend (b_2)	9	87.5	+10.0	97.5	0.07836	−0.0000484	0.0000502
			V$^+$(H$_2$O)				
O−H sym. stretch	1	3794.3	−182.0	3612.3	0.24162	−0.0000878	0.0000031
H$_2$O scissor	2	1679.3	−43.6	1635.7	−0.17069	−0.0002382	0.0001265
V−O stretch	3	407.3	−11.1	396.2	−0.00674	0.0030815	0.0030579
H$_2$O wag	4	265.3	+120.5	385.8	1.86054	−0.0001442	−0.0007827
O−H antisym. stretch	5	3878.5	−197.3	3681.2	0.14051	−0.0000800	−0.0000583
H$_2$O rock	6	552.7	−3.3	549.4	−1.46988	−0.0001857	0.0003552
			H$_2$O				
O−H sym. stretch	1	3831.7	−176.7	3655.0	0.63733	0.2230477	0.1724306
H$_2$O scissor	2	1639.3	−43.3	1596.0	−2.56400	−0.1529430	0.1405468
O−H antisym. stretch	3	3942.6	−189.8	3752.9	1.12194	0.0948105	0.1396034

^{a} Harmonic frequencies (ω_i), total anharmonicities (Δ_i), fundamental frequencies (ν_i), and vibration−rotation interaction constants (α_i^A, α_i^B, α_i^C) for $^5A_1$ state of ^{40}Ar^{51}V$^+$(H$_2^{16}$O), ^{51}V$^+$(H$_2^{16}$O), and H$_2^{16}$O in cm^{-1}. No strong anharmonic resonances required exclusion. The $\omega_6-\omega_9$ Coriolis resonance was removed in computing the α_i constants of ArV$^+$(H$_2$O).

of the equilibrium structures, giving rise to near singularities in the $^5B_1$ force field expansion for ArV$^+$(H$_2$O).

In Tables S2 and S3 of Supporting Information, the Wf(TZP) CCSD and CCSD(T) quartic force fields are given for the $^5A_1$ ground state of V$^+$(H$_2$O), along with the CCSD/Wf(TZP) force field for the analogous $^5A_1$ state of ArV$^+$(H$_2$O). For comparison, the Wf(TZP) CCSD and CCSD(T) quartic force fields of free H$_2$O are given in Table S4. No anomalous force constants occur for ArV$^+$(H$_2$O) in the $^5A_1$ state, in contrast to its close-lying $^5B_1$ counterpart. Therefore, our analysis of vibrational anharmonicity in the V$^+$(H$_2$O) and ArV$^+$(H$_2$O) species centers on the $^5A_1$ electronic state throughout. The issues of concern here can be addressed via a VPT2 treatment based on quartic force fields, although it must be recognized that a rigorous analysis would entail a detailed variational treatment of nonadiabatic vibrational phenomena. In essence, we focus here on inherent (adiabatic) anharmonic vibrational effects unspoiled by vibronic coupling within the manifold of low-lying quintet electronic states.

The VPT2 anharmonicities (Δ_i) and vibration−rotation interaction constants (α_i) of ArV$^+$(H$_2$O), V$^+$(H$_2$O), and free H$_2$O are compared in Table 8, at a common level of theory [CCSD/Wf(TZP)]. Corresponding results for five sets of isotopic derivatives of these species are given in Supporting Information Tables S5−S8. Finally, CCSD(T)/Wf(TZP) anharmonicities for V$^+$(H$_2$O) and H$_2$O are provided in Supporting Information Table S9. We investigated the influence of a number of potential anharmonic resonances on the fundamental frequencies of the isotopologs. The exclusion of resonance interactions based on a 20 cm^{-1} cutoff for zeroth-order state separations changed the computed VPT2 anharmonicities by more than 1 cm^{-1} in only one case: the $2\omega_5$(H$_2$O wag) − ω_3(V−O stretch) Fermi resonance in ^{40}Ar^{51}V$^+$(D$_2$O). Thus, in our tabulated results, no anharmonic resonances were removed, except for the $2\omega_5-\omega_3$ interaction in ^{40}Ar^{51}V$^+$(D$_2$O) (Table S5). The ω_6[Ar−V−O linear bend (b_1)] − ω_9[Ar−V−O linear bend (b_2)] Coriolis resonance has a strong influence on the α_6^A and α_9^A constants for all ArV$^+$(H$_2$O) isotopologs. Exclusion of this interaction from the VPT2 treatment was necessary to obtain valid vibration−rotation interaction constants in all cases, but the

overall ZPV shift on the rotational constants is completely invariant to the removal of such Coriolis resonances.

The theoretical fundamental frequencies of H$_2$O (Table 8) lie within a few inverse centimeters of the observed band origins for the parent isotopolog, $\nu_1 = 3657.1$, $\nu_2 = 1594.7$, and $\nu_3 = 3755.9$ cm^{-1}.[92,93] Thus, the CCSD/Wf(TZP) method is providing a particularly advantageous balance of errors in the electronic structure treatment. The CCSD/Wf(TZP) O−H stretching anharmonicities are equally well matched with experiment ($\Delta_1 = -173$ cm^{-1}, $\Delta_3 = -185$ cm^{-1}),[94−96] whereas the computed anharmonicity for the H$_2$O scissor is about 12 cm^{-1} smaller in magnitude than the empirically derived value ($\Delta_2 = -55$ cm^{-1}).[94−96]

Formation of the V$^+$(H$_2$O) complex increases the magnitude of the O−H stretching anharmonicities by 5−8 cm^{-1}, while leaving the scissoring anharmonicity unaffected. The interfragment V−O stretching and H$_2$O rocking modes of V$^+$(H$_2$O) have small anharmonicities of −11 cm^{-1} and −3 cm^{-1}, respectively. In contrast, the H$_2$O wag has an enormous anharmonicity in the positive direction ($\Delta_4 = +120$ cm^{-1}), displaying strong characteristics of a quartic oscillator.

Argon tagging (without electronic state switching) has remarkably little effect (1.3 cm^{-1} on average) on the vibrational anharmonicities of V$^+$(H$_2$O), including the large positive value for the H$_2$O wag. The anharmonicity of the newly formed Ar−V stretching mode is only −7.5 cm^{-1}. On the other hand, the Ar−V−O linear bends $\nu_6(b_1)$ and $\nu_9(b_2)$ have proportionally large anharmonicities of +21.7 and +10.0 cm^{-1}, respectively. These sizable, positive values can be directly traced to the large rotational A_e constant of the ArV$^+$(H$_2$O) adduct and the associated Coriolis contributions $[A_e(\zeta_{rs}^a)^2(\omega_r/\omega_s + \omega_s/\omega_r)]$ to the off-diagonal χ_{rs} anharmonicity constants.

The vibration−rotation interaction constants (α_i) are of particular interest here, because they allow a determination of zero-point vibrational effects on the geometric structures of V$^+$(H$_2$O) and ArV$^+$(H$_2$O). As shown in Table 8, the binding of the vanadium cation to water has dramatic effects on the α_i constants of the H$_2$O vibrational modes. In contrast, further argon tagging of V$^+$(H$_2$O) has no significant effect, particularly

for the all-important α_i^A constants. For the α_i^B and α_i^C parameters, argon complexation merely reduces the magnitude of these already-small vibration−rotation interaction constants.

A key question is whether some of the disparity between the water bond angle widening in V$^+$(H$_2$O) theoretically predicted here (2−3°) and that surmised from the IRPD experiments in the Duncan laboratory[21] (9.3°) can be attributed to zero-point vibrational effects on the effective geometric structure. In the equilibrium structures of V$^+$(H$_2$O) and ArV$^+$(H$_2$O), only the light hydrogen atoms contribute to the A rotational constants; however, vibrational motion along the b_1 and b_2 modes displaces the massive vanadium and/or argon atoms off the a principal axis, potentially increasing the effective I_A moment of inertia by a substantial amount. To investigate this effect, we used our CCSD/Wf(TZP) α_i constants to synthesize (A_0, B_0, C_0) rotational constants for several isotopologs of V$^+$(H$_2$O) and ArV$^+$(H$_2$O) and then to extract vibrationally averaged r_0 structures by least-squares fits. The molecular structure refinements were performed using a robust computer program MolStruct recently developed by one of us.[97] The following V$^+$(H$_2$O) isotopologs were employed in the least-squares refinment: (^{51}V, ^{16}O, H, H), (^{51}V, ^{18}O, H, H), (^{51}V, ^{16}O, D, D), and (^{50}V, ^{16}O, H, H). For ArV$^+$(H$_2$O), the same isotopologs were used with ^{40}Ar included, and one more isotopolog was added: (^{36}Ar, ^{51}V, O, H, H). All the necessary vibration−rotation interaction constants appear in Table 8 and Supporting Information Tables S5−S8. Our best CCSD(T)/QZVPP equilibrium geometries were employed as reference structures for the determination of $r_e − r_0$ shifts. We found that the standard errors of the r_0 fits were significantly reduced by excluding the A_0 rotational constants from the refinements, so unless otherwise stated, only the much smaller (B_0, C_0) values were included in the MolStruct data set.

Our vibrationally averaged structural parameters for the $^5A_1$ state of V$^+$(H$_2$O) differ from the equilibrium structural parameters by the following amounts: θ_0(H−O−H) − θ_e(H−O−H) = +2.35°, r_0(O−H) − r_e(O−H) = +0.0025 Å, and r_0(V−O) − r_e(V−O) = +0.0066 Å. If the A_0 rotational constants are included in the refinement, then θ_0(H−O−H) − θ_e(H−O−H) = +1.82°, r_0(O−H) − r_e(O−H) = −0.0018 Å, and r_0(V−O) − r_e(V−O) = +0.0066 Å, still showing a substantial angle expansion. If the interfragment modes of V$^+$(H$_2$O) are excluded from the vibrational averaging by omitting all α_3, α_4, and α_6 constants, then θ_0(H−O−H) − θ_e(H−O−H) = +0.40° and r_0(O−H) − r_e(O−H) = +0.0146 Å. Császár and co-workers[98] have very recently published effective rotational constants (A_0, B_0, C_0) of water isotopologs arising from variational vibrational computations on the near spectroscopic quality, empirically adjusted CVRQD potential energy surface.[99] Applying our MolStruct procedure to these (A_0, B_0, C_0) rotational constants yields the following shifts for free H$_2$O from the highly accurate CVRQD water surface: r_0(O−H) − r_e(O−H) = +0.0025 Å and θ_0(H−O−H) − θ_e(H−O−H) = +0.69°. An analogous refinement using our Wf(TZP) CCSD α_i constants for free water instead of the CVRQD vibrational corrections of ref 98 gives r_0(O−H) − r_e(O−H) = +0.0029 Å and θ_0(H−O−H) − θ_e(H−O−H) = +0.64°. Finally, for the $^5A_1$ state of ArV$^+$(H$_2$O), we find θ_0(H−O−H) − θ_e(H−O−H) = 2.08°, r_0(O−H) − r_e(O−H) = −0.007 Å, r_0(V−O) − r_e(V−O) = +0.005 Å, and r_0(Ar−V) − r_e(Ar−V) = +0.011 Å.

The primary conclusions to be derived from our r_0 structural data are the following: (1) the results for free H$_2$O indicate the validity of performing MolStruct r_0 fits based on Wf(TZP) CCSD vibration−rotation interaction constants; (2) zero-point vibrational averaging in V$^+$(H$_2$O) widens the H−O−H bond

angle by 2.4°, and argon tagging reduces this shift by about +0.3°; (3) most of the ZPV effect on the H−O−H angle is due to off-axis motions of the massive V atom rather than to flattening of the potential energy curve for H$_2$O bending resulting from complexation with the vanadium cation; and (4) adding the computed effects of vibrational averaging to our best equilibrium structures [CCSD(T)/QZVPP] for the ground states of V$^+$(H$_2$O) and ArV$^+$(H$_2$O) gives θ_0(H−O−H) angles of 109.1° and 108.7°, respectively. The H$_2$O bond angle value derived from the IRPD experiments (113.8°)[21] is still about 5° higher than that predicted by our high-level theoretical analysis; however, consideration of zero-point vibrational effects has lowered this disparity by 2−3°. The remaining discrepancy is evident by directly comparing our best purely theoretical A_0 rotational constants for the $^5A_1$ states of V$^+$(H$_2$O) and ArV$^+$(H$_2$O) (13.70 cm^{-1} and 13.65 cm^{-1}, respectively) with the significantly smaller IRPD value (12.52 cm^{-1}).[21]

IV. Conclusions

The model systems V$^+$(H$_2$O) and ArV$^+$(H$_2$O), exemplary of mass-selected infrared photodissociation (IRPD) spectroscopy on hydrated metal cations, have been thoroughly investigated by high-level electronic structure theory. Our best predictions are based on restricted open-shell CCSD(T) theory implemented with a massive V[11s6p5d3f2g], Ar[9s6p4d2f1g], O[6s5p4d3f2g], and H[5s4p3d2f] (QZVPP) basis set and with the outer-core V(3s,3p) electrons correlated. The microsolvation of V$^+$ with one water molecule gives an equilibrium V−O distance of 2.049 Å and a binding energy (D_0) of 36.2 kcal mol^{-1}. Formation of the V$^+$(H$_2$O) complex shifts the H$_2$O fundamentals (ν_1, ν_2, ν_3) by (−43, +26, −72) cm^{-1}. Our computed red shifts for the O−H stretching modes (ν_1, ν_3) are in excellent agreement with the IRPD results (∼50, ∼70) cm^{-1} from the Duncan laboratory.[21] When H$_2$O binds to V$^+$, the H−O−H equilibrium bond angle widens by +2.4°, with a concomitant increase in the O−H distance of +0.004 Å. The H$_2$O molecule splits the degenerate ground-state manifold of V$^+$(^5D), yielding electronic states in C_{2v} symmetry with the following relative energies: T_e($^5A_1$, $^5A_2$, $^5B_1$, $^5B_2$) = (0, 0.15, 0.37, 5.09) kcal mol^{-1}. A second $^5A_1$ state of V$^+$(H$_2$O) appears somewhat higher in energy, and the lowest-lying triplet state is more than 15 kcal mol^{-1} above the ground $^5A_1$ state.

Argon tagging of V$^+$(H$_2$O) places the Ar atom 2.538 Å from the V$^+$ center and 180° removed from the H$_2$O ligand, in accord with simple expectation for an electrostatic complex. The argon binding energy is D_0[Ar−V$^+$(H$_2$O)] = 9.4 kcal mol^{-1}. Virtually none of this binding energy is obtained with Hartree−Fock theory, which yields only a 0.25 kcal mol^{-1} stabilization even with the large QZVPP basis set. Argon tagging engenders only small perturbations in the V$^+$(H$_2$O) structure: δr_e(V−O) = −0.0105 Å, δr_e(O−H) = +0.0003 Å, and $\delta\theta_e$(H−O−H) = −0.14°. However, the Ar "spectator" is responsible for a number of subtle effects, such as switching the electronic ground state. For ArV$^+$(H$_2$O), our best theory predicts a $^5B_1$ ground state and excitation energies T_e($^5A_1$, $^5A_2$, $^5B_2$) = (0.49, 0.62, 4.17) kcal mol^{-1}. Argon tagging shifts the vibrational frequencies of V$^+$(H$_2$O) by no more than 10 cm^{-1}, but the direction of the shift is in most cases dependent on whether the final electronic state in question is $^5A_1$ or $^5B_1$.

An analysis of vibrational anharmonicity effects in V$^+$(H$_2$O) and ArV$^+$(H$_2$O) has been executed by computing complete quartic force fields and then applying second-order vibrational

V$^+$(H$_2$O) and ArV$^+$(H$_2$O) Complexes

J. Phys. Chem. A, Vol. 111, No. 31, 2007 **7609**

perturbation theory (VPT2) to determine anharmonic constants and vibration−rotation interaction constants. This approach probes inherent anharmonic vibrational properties of single electronic states in these species. Rigorous variational computations of the vibronic coupling in these systems are not currently practical. For free H$_2$O, our quartic force fields reproduce the observed O−H stretching fundamentals to within 5 cm^{-1}, bolstering confidence in our analogous results for V$^+$(H$_2$O) and ArV$^+$(H$_2$O). Our vibration−rotation interaction constants allow quantification of the influence of zero-point vibrational (ZPV) averaging on the molecular structures of V$^+$(H$_2$O) and ArV$^+$(H$_2$O). A peculiar phenomenon is observed for the *effective* bond angle θ_0(H−O−H), specifically, a ZPV increase of 2−3° as a consequence of off-axis motion of the heavy vanadium atom, as opposed to flattening and/or skewing of the water bending potential. Nonetheless, the total complexation effect on the water bond angle computed here (about +4°) is substantially less than the 9° widening surmised from the IRPD experiments.[21] Thermal averaging over excited vibrational states in the V$^+$(H$_2$O) and ArV$^+$(H$_2$O) complexes might increase the effective H−O−H angle more and further reduce the disparity between theory and experiment. However, it is clear that the interpretation of geometric parameters extracted from IRPD profiles is complicated by numerous effects, and thus, care must be taken in equating effective bond angle widening with changes in electronic structure upon complexation.

A number of issues of theoretical interest were encountered in our study of V$^+$(H$_2$O) and ArV$^+$(H$_2$O): (1) The V$^+$(H$_2$O) binding energy appears to be very sensitive to vanadium (3s,3p) core electron correlation. (2) There is large quartic anharmonicity in the H$_2$O wagging mode in V$^+$(H$_2$O) and ArV$^+$(H$_2$O). (3) Curve crossings within the lowest-lying quintet manifold of ArV$^+$(H$_2$O) occur near the equilibrium geometry, giving rise to anomalous force constants in the local representations of the potential energy surfaces of some of the electronic states. These crossings arise along the Ar−V stretching mode and thus are precipitated by the presence of the argon "spectator" atom. (4) Finally, the intricate vibronic coupling within the ($^5A_1$, $^5A_2$, $^5B_1$, $^5B_2$) manifold of V$^+$(H$_2$O) and ArV$^+$(H$_2$O) remains unexplored. All of these issues would be worthy targets of future investigations.

Supporting Information Available: Quartic force fields of V$^+$(H$_2$O), ArV$^+$(H$_2$O), and H$_2$O, as well as summaries of anharmonic vibrational analyses of isotopologs of these species. This material is available free of charge via the Internet at http://pub.acs.org.

References and Notes

(1) Lessen, D. E.; Asher, R. L.; Brucat, P. J. *J. Chem. Phys.* **1990**, *93*, 6102.

(2) Willey, K. F.; Yeh, C. S.; Robbins, D. L.; Pilgrim, J. S.; Duncan, M. A. *J. Chem. Phys.* **1992**, *97*, 8886.

(3) Scurlock, C. T.; Pullins, S. H.; Reddic, J. E.; Duncan, M. A. *J. Chem. Phys.* **1996**, *104*, 4591.

(4) Duncan, M. A. *Annu. Rev. Phys. Chem.* **1997**, *48*, 69.

(5) Sanekata, M.; Misaizu, F.; Fuke, K. *J. Chem. Phys.* **1996**, *104*, 9768.

(6) Misaizu, F.; Sanekata, M.; Tsukamoto, K.; Fuke, K.; Iwata, S. *J. Phys. Chem.* **1992**, *96*, 8259.

(7) Fuke, K.; Hashimoto, K.; Iwata, S. *Adv. Chem. Phys.* **1999**, *110*, 431.

(8) Abate, Y.; Kleiber, P. D. *J. Chem. Phys.* **2005**, *122*, 084305.

(9) Thompson, C. J.; Husband, J.; Aguirre, F.; Metz, R. B. *J. Phys. Chem. A* **2000**, *104*, 8155.

(10) Faherty, K. P.; Thompson, C. J.; Aguirre, F.; Michne, J.; Metz, R. B. *J. Phys. Chem. A* **2001**, *105*, 10054.

(11) Thompson, C. J.; Aguirre, F.; Husband, J.; Metz, R. B. *J. Phys. Chem. A* **2000**, *104*, 9901.

(12) Agreiter, J. K.; Knight, A. M.; Duncan, M. A. *Chem. Phys. Lett.* **1999**, *313*, 162.

(13) Lisy, J. M. *Int. Rev. Phys. Chem.* **1997**, *16*, 267.

(14) Cabarcos, O. M.; Weinheimer, C. J.; Lisy, J. M. *J. Chem. Phys.* **1998**, *108*, 5151.

(15) Cabarcos, O. M.; Weinheimer, C. J.; Lisy, J. M. *J. Chem. Phys.* **1999**, *110*, 8429.

(16) Vaden, T. D.; Forinash, B.; Lisy, J. M. *J. Chem. Phys.* **2002**, *117*, 4628.

(17) Gregoire, G.; Duncan, M. A. *J. Chem. Phys.* **2002**, *117*, 2120.

(18) van Heijnsbergen, D.; von Helden, G.; Meijer, G.; Maitre, P.; Duncan, M. A. *J. Am. Chem. Soc.* **2002**, *124*, 1562.

(19) Walters, R. S.; Jaeger, T.; Duncan, M. A. *J. Phys. Chem. A* **2002**, *106*, 10482.

(20) Duncan, M. A. *Int. Rev. Phys. Chem.* **2003**, *22*, 407.

(21) Walker, N. R.; Walters, R. S.; Pillai, E. D.; Duncan, M. A. *J. Chem. Phys.* **2003**, *119*, 10471. Note: The basis set used for the DFT computations in this reference was 6-31G*; due to a typographical error, the basis set is reported as 3-31G* therein.

(22) Jaeger, T.; Pillai, E. D.; Duncan, M. A. *J. Phys. Chem. A* **2004**, *108*, 6605.

(23) Walker, N. R.; Walters, R. S.; Duncan, M. A. *J. Chem. Phys.* **2004**, *120*, 10037.

(24) Walker, N. R.; Walters, R. S.; Grieves, G. A.; Duncan, M. A. *J. Chem. Phys.* **2004**, *121*, 10498.

(25) Walters, R. S.; Duncan, M. A. *Aust. J. Chem.* **2003**, *57*, 1145.

(26) Walker, N. R.; Walters, R. S.; Tsai, M.-K.; Jordan, K. D.; Duncan, M. A. *J. Phys. Chem. A* **2005**, *109*, 7057.

(27) Walters, R. S.; Pillai, E. D.; Duncan, M. A. *J. Am. Chem. Soc.* **2005**, *127*, 16599.

(28) Inokuchi, Y.; Ohshimo, K.; Misaizu, F.; Nishi, N. *J. Phys. Chem.* **2004**, *108*, 5034.

(29) Inokuchi, Y.; Ohshimo, K.; Misaizu, F.; Nishi, N. *Chem. Phys. Lett.* **2004**, *390*, 140.

(30) *Organometallic Ion Chemistry*; Freiser, B. S., Ed.; Kluwer: Dordrecht, The Netherlands, 1996.

(31) Magnera, T. F.; David, D. E.; Michl, J. *J. Am. Chem. Soc.* **1989**, *111*, 4100.

(32) Marinelli, P. J.; Squires, R. R. *J. Am. Chem. Soc.* **1989**, *111*, 4101.

(33) Clemmer, D. E.; Chen, Y.-M.; Aristov, N.; Armentrout, P. B. *J. Phys. Chem.* **1994**, *98*, 7538.

(34) Dalleska, N. F.; Honma, K.; Sunderlin, L. S.; Armentrout, P. B. *J. Am. Chem. Soc.* **1994**, *116*, 3519.

(35) *Gas Phase Metal Ion Chemistry*; Leary, J. A.; Armentrout, P. B., Ed.; special issue of *Int. J. Mass. Spectrom.* **2001**, *204*, 1.

(36) Duncan, M. A. *Adv. Met. Semicond. Clusters* **2002**, *5*.

(37) Armentrout, P. B. *Int. J. Mass. Spectrom.* **2003**, *227*, 289.

(38) Schröder, D.; Engeser, M.; Schwarz, H.; Harvey, J. N. *ChemPhysChem* **2002**, *3*, 584.

(39) Lessen, D.; Brucat, P. J. *J. Chem. Phys.* **1989**, *91*, 4522.

(40) Rosi, M.; Bauschlicher, C. W., Jr. *J. Chem. Phys.* **1989**, *90*, 7264.

(41) Rosi, M.; Bauschlicher, C. W., Jr. *J. Chem. Phys.* **1990**, *92*, 1876.

(42) Magnusson, E.; Moriarty, N. W. *J. Comp. Chem.* **1993**, *14*, 961.

(43) Trachtman, M.; Markham, G. D.; Glusker, J. P.; George, P.; Bock, C. W. *Inorg. Chem.* **1998**, *37*, 4421.

(44) Irigoras, A.; Fowler, J. E.; Ugalde, J. M. *J. Am. Chem. Soc.* **1999**, *121*, 574.

(45) Klippenstein, S. J.; Yang, C.-N. *Int. J. Mass Spectrom.* **2000**, *201*, 253.

(46) Dunbar, R. C. *J. Phys. Chem. A* **2002**, *106*, 7328.

(47) Roothaan, C. C. J. *Rev. Mod. Phys.* **1951**, *23*, 69.

(48) Pople, J. A.; Nesbet, R. K. *J. Chem. Phys.* **1954**, *22*, 571.

(49) Hehre, W. J.; Radom, L.; Schleyer, P. v. R.; Pople, J. A. *Ab initio Molecular Orbital Theory*; Wiley-Interscience: New York, 1986.

(50) Szabo, A.; Ostlund, N. S. *Modern Quantum Chemistry: Introduction to Advanced Electronic Structure Theory*, 1st ed. revised; McGraw-Hill: New York, 1989.

(51) Purvis, G. D., III; Bartlett, R. J. *J. Chem. Phys.* **1982**, *76*, 1910.

(52) Scuseria, G. E.; Scheiner, A. C.; Lee, T. J.; Rice, J. E.; Schaefer, H. F., III. *J. Chem. Phys.* **1987**, *86*, 2881.

(53) Rittby, M.; Bartlett, R. J. *J. Phys. Chem.* **1988**, *92*, 3033.

(54) Knowles, P. J.; Hampel, C.; Werner, H.-J. *J. Chem. Phys.* **1993**, *99*, 5219.

(55) Raghavachari, K.; Trucks, G. W.; Pople, J. A.; Head-Gordon, M. *Chem. Phys. Lett.* **1989**, *157*, 479.

(56) Bartlett, R. J.; Watts, J. D.; Kucharski, S. A.; Noga, J. *Chem. Phys. Lett.* **1990**, *165*, 513.

Kasalová et al.

(57) Bartlett, R. J.; Watts, J. D.; Kucharski, S. A.; Noga, J. *Chem. Phys. Lett.* **1990**, *167*, 609.

(58) Watts, J. D.; Gauss, J.; Bartlett, R. J. *J. Chem. Phys.* **1993**, *98*, 8718.

(59) Knowles, P. J.; Werner, H.-J. *Chem. Phys. Lett.* **1985**, *115*, 259.

(60) Werner, H.-J.; Knowles, P. J. *J. Chem. Phys.* **1985**, *82*, 5053.

(61) Wachters, A. J. H. *J. Chem. Phys.* **1970**, *52*, 1033.

(62) Basis sets were obtained from the Extensible Computational Chemistry Environment Basis Set Database, Version 02/25/04, as developed and distributed by the Molecular Science Computing Facility, Environmental and Molecular Sciences Laboratory which is part of the Pacific Northwest Laboratory, P.O. Box 999, Richland, Washington 99352, U.S.A. and funded by the U.S. Department of Energy. The Pacific Northwest Laboratory is a multi-program laboratory operated by Battelle Memorial Institute for the U.S. Department of Energy under contract DE-AC06−76RLO 1830. Contact Karen Schuchardt for further information.

(63) Bauschlicher, C. W., Jr.; Langhoff, S. R.; Barnes, L. A. *J. Chem. Phys.* **1989**, *91*, 2399.

(64) Hay, P. J. *J. Chem. Phys.* **1977**, *66*, 4377.

(65) Dunning, T. H., Jr. *J. Chem. Phys.* **1971**, *55*, 716.

(66) Schäfer, A.; Huber, C.; Ahlrichs, R. *J. Chem. Phys.* **1994**, *100*, 5829.

(67) Schäfer, A.; Horn, H.; Ahlrichs, R. *J. Chem. Phys.* **1992**, *97*, 2571.

(68) Weigend, F.; Furche, F.; Ahlrichs, R. *J. Chem. Phys.* **2003**, *119*, 12753.

(69) Dunning, T. H., Jr. *J. Chem. Phys.* **1989**, *90*, 1007.

(70) Kendall, R. A.; Dunning, T. H., Jr.; Harrison, R. J. *J. Chem. Phys.* **1992**, *96*, 6796.

(71) Nielsen, H. H. *Rev. Mod. Phys.* **1951**, *23*, 90.

(72) Watson, J. K. G. In *Vibrational Spectra and Structure*; Durig, J. R., Ed.; Elsevier: Amsterdam, The Netherlands, 1997; Vol. 6, p 1.

(73) Papoušek, D.; Aliev, M. R. *Molecular Vibrational-Rotational Spectra*; Elsevier: Amsterdam, The Netherlands, 1982.

(74) Allen, W. D.; Yamaguchi, Y.; Császár, A. G.; Clabo, D. A., Jr.; Remington, R. B.; Schaefer, H. F., III. *Chem. Phys.* **1990**, *145*, 427.

(75) Clabo, D. A., Jr.; Allen, W. D.; Remington, R. B.; Yamaguchi, Y.; Schaefer, H. F., III. *Chem. Phys.* **1988**, *123*, 187.

(76) East, A. L. L.; Johnson, C. S.; Allen, W. D. *J. Chem. Phys.* **1993**, *98*, 1299.

(77) INTDIF2005 is an abstract program written by Wesley D. Allen for *Mathematica* (Wolfram Research, Inc., Champaign, IL) to perform general numerical differentiation to high orders of electronic structure data.

(78) DeKock, R. L.; McGuire, M. J.; Piecuch, P.; Allen, W. D.; Schaefer, H. F., III.; Kowalski, K.; Kucharski, S. A.; Musial, M.; Bonner, A. R.; Spronk, S. A.; Lawson, D. B.; Laursen, S. L. *J. Phys. Chem. A* **2004**, *108*, 2893.

(79) INTDER2005 is a general program written by W. D. Allen which performs sundry vibrational analyses and higher-order nonlinear transformations among force field representations.

(80) Allen, W. D.; Császár, A. G. *J. Chem. Phys.* **1993**, *98*, 2983.

(81) Allen, W. D.; Császár, A. G.; Szalay, V.; Mills, I. M. *Mol. Phys.* **1996**, *89*, 1213.

(82) See program descriptions: Sarka, K.; Demaison, J. In *Computational Molecular Spectroscopy*, Jensen, P., Bunker, P. R., Eds.; Wiley: Chichester, 2000; p 255.

(83) ANHARM is a FORTRAN program written for VPT2 analyses by Yukio Yamaguchi and Henry F. Schaefer (Center for Computational Chemistry, University of Georgia, Athens, GA, 30602).

(84) Stanton, J. F.; Gauss, J.; Watts, J. D.; Szalay, P. G.; Bartlett, R. J. with contributions from Auer, A. A.; Bernholdt, D. B.; Christiansen, O.; Harding, M. E.; Heckert, M.; Heun, O.; Huber, C.; Jonsson, D.; Jusélius, J.; Lauderdale, W. J.; Metzroth, T.; Michauk, C.; Ruud, K.; Schiffmann, F.; Tajti, A. and the integral packages: MOLECULE (J. Almlöf and P.R. Taylor), PROPS (P.R. Taylor), and ABACUS (T. Helgaker, H. J. Aa. Jensen, P. Jørgensen, and J. Olsen). See also Stanton, J. F.; Gauss, J.; Watts, J. D.; Lauderdale, W. J.; Bartlett, R. J. *Int. J. Quantum Chem. Symp.* **1992**, *26*, 879. Current version see http://www.aces2.de.

(85) Werner, H.-J.; Knowles, P. J.; Schütz, M.; Lindh, R.; Celani, P.; Korona, T.; Rauhut, G.; Manby, F. R.; Amos, R. D.; Bernhardsson, A.; Berning, A.; Cooper, D. L.; Deegan, M. J. O.; Dobbyn, A. J.; Eckert, F.; Hampel, C.; Hetzer, G.; Lloyd, A. W.; McNicholas, S. J.; Meyer, W.; Mura, M. E.; Nicklass, A.; Palmieri, P.; Pitzer, R. M.; Schumann, U.; Stoll, H.; Stone, A. J.; Tarroni, R.; Thorsteinsson, T. *MOLPRO*, version 2002.1; Birmingham, U.K., 2003.

(86) Balasubramanian, K. *Relativistic Effects in Chemistry: Part A, Theory and Techniques;* Wiley: New York, 1997.

(87) Balasubramanian, K. *Relativistic Effects in Chemistry: Part B, Applications;* Wiley: New York, 1997.

(88) Cowan, R. D.; Griffin, D. C. *J. Opt. Soc. Am.* **1976**, *66*, 1010.

(89) Perera, S. A.; Bartlett, R. J. *Chem. Phys. Lett.* **1993**, *252*, 425.

(90) Tarczay, G.; Császár, A. G.; Klopper, W.; Quiney, H. M. *Mol. Phys.* **2001**, *99*, 1769.

(91) Moore, C. E. *Atomic Energy Levels;* National Bureau of Standards, Circ. 467; Vol. 1.

(92) Camy-Peyret, C.; Flaud, J.-M.; Maillard, J.-P.; Guelachvili, G. *Mol. Phys.* **1977**, *33*, 1641.

(93) Pugh, L. A.; Narahari Rao, K. *J. Mol. Spectrosc.* **1973**, *47*, 403.

(94) Benedict, W. S.; Gailar, N.; Plyler, E. K. *J. Chem. Phys.* **1956**, *24*, 1139.

(95) Plíva, J.; Špirko, V.; Papoušek, D. *J. Mol. Spectrosc.* **1967**, *23*, 331.

(96) Császár, A. G.; Mills, I. M. *Spectrochim. Acta* **1997**, *53A*, 1101.

(97) MolStruct is an abstract program developed by Wesley D. Allen for use within *Mathematica* (Wolfram Research Inc., Champaign, Illinois) to perform diverse fits of molecular structures to sets of isotopologic rotational constants.

(98) Császár, A. G.; Czakó, G.; Furtenbacher, T.; Tennyson, J.; Szalay, V.; Shirin, S. V.; Zobov, N. F.; Polyansky, O. L. *J. Chem. Phys.* **2005**, *122*, 214305.

(99) Polyansky, O. L.; Császár, A. G.; Shirin, S. V.; Zobov, N. F.; Barletta, P.; Tennyson, J.; Schwenke, D. W.; Knowles, P. J. *Science* **2003**, *299*, 539.

(100) Barletta, P.; Shirin, S. V.; Zobov, N. F.; Polyanksy, O. L.; Tennyson, J.; Valeev, E. F.; Császár, A. G. *J. Chem. Phys.* **2006**, *125*, 204307.